Strength Analysis of a Composite Turbine Blade Using Puck Failure Criteria

IOP Conf. Series: Journal of Physics: Conf. Series **1037** (2018) 042027 doi:10.1088/1742-6596/1037/4/042027

Strength Analysis of a Composite Turbine Blade Using Puck Failure Criteria

M Ozyildiz[1], C Muyan[1], D Coker[2]

[1] Graduate Student, Dept. of Aerospace Engineering, METU, 06800 Ankara/TURKEY
[2] Associate Professor, Dept. of Aerospace Engineering, Director, Structures and Materials Laboratories, RUZGEM, METU Center for Wind Energy, 06800 Ankara/TURKEY

E-mail: coker@metu.edu.tr

Abstract. The strength analysis of an existing 5-meter composite wind turbine blade using Tsai-Wu and Puck failure criteria is presented. Finite element analysis is performed on the blade under static flap wise loading. ANSYS APDL scripting language is used to implement Puck failure criteria and degradation rules for the progressive failure analysis of the blade. Evaluation and visualization of Tsai-Wu inverse reserve factors and Puck failure exposures in the blade is done with the help of the Ansys ACP/Post module. The results of this study indicate that the blade is not able resist extreme load case and needs to be redesigned. Root and trailing edge of the blade have the highest risk of failure initiation. Linear analysis using Tsai-Wu and Puck failure criteria is compared with the nonlinear analysis using progressive Puck failure criteria. It is concluded that progressive analysis is necessary for a more realistic simulation of blade failure mechanisms. Results of the analysis will be used to calibrate structural test set-up of the blade.

1. Introduction

The long-term reliability of wind turbines is very important for sustainable and economically viable wind energy utilization. Therefore, wind turbine designs must be optimized to minimize costs and maximize lifetime. This requires performance and durability characteristics of wind turbine materials, components and structures to be understood extensively. The most critical component of a wind turbine is the composite rotor blade. A rotor blade failure can have a significant impact on turbine downtime and safety. To avoid a blade failure, knowing the strength of the composite rotor blades is essential. Hence, validation of a composite blade resistance must be checked by structural testing and/or analysis [1]. However, the structural testing methods such as full-scale testing of the blade are expensive and troublesome due to construction of a test set-up. In order to provide more data for structural design and analysis of wind turbine blades, test approaches are being developed [2]. Structural analyses are utilized to calibrate structural blade test set-ups for different loading scenarios.

In the literature, there are many studies on the structural behaviour of composite wind turbine blades. For instance, a novel methodology for the structural design and analysis of tidal turbine blade is presented based on the Puck phenomenological failure criteria for fibre and inter-fibre failure [3]. The methodology that is developed in the study predicted damage values for different load cases. This methodology is an iterative design process with respect to failure criteria to check structural strength of the blade. Another study developed is a fatigue damage simulator utilizing the failure criteria and degradation rules of Puck for the life prediction of composites under variable amplitude loading [4]. Puck failure criteria are used to predict failure initiation and sudden stiffness degradation. In another article, structural analysis was performed using finite element method to evaluate a proposed medium scale composite wind turbine blade [5]. The fatigue life of that blade was estimated by using the well-known S–N linear damage theory, the service load spectrum, and the Spera's empirical equations. The results show that the most dominant parameters in the blade are the thickness of spar flange and skin for minimization of weight, the thickness and the location of spar webs for maximum stress and strain.

Another study is on a full-scale 34-meter composite wind turbine blade test to check failure under flap-wise loading and simulated using finite element analysis [6]. The test results show that typical damage modes occur in the aeroshell and spar including delamination between composite plies and debonding along adhesive joints.

The objective of this paper is to develop a finite element model to analyse an existing 5-meter wind turbine blade to predict the strength of the blade utilizing Puck Failure Criteria under static loading. This analysis is going to be used to predict failure initiation load, failure modes and their locations before the structural testing. Results from finite element analysis are going to be utilized to calibrate structural test set-up for investigating structural behaviour of the blade under different loading scenarios.

The existing blade was designed as part of a project between RUZGEM – METU Center for Wind Energy and Core Team of the University of PATRAS according to IEC 61400-2 [7]. The blade was designed for a wind turbine that has 30 kW nominal power capacity at 10 m/s wind speed. According to the wind turbine characteristics, the blade optimized aerodynamic and geometric design was finalized by the blade manufacturer. The existing blade consists of five main parts: suction side, pressure side, internal flange, “hat shaped” chassis/spar, and flange as seen in Figure 1.

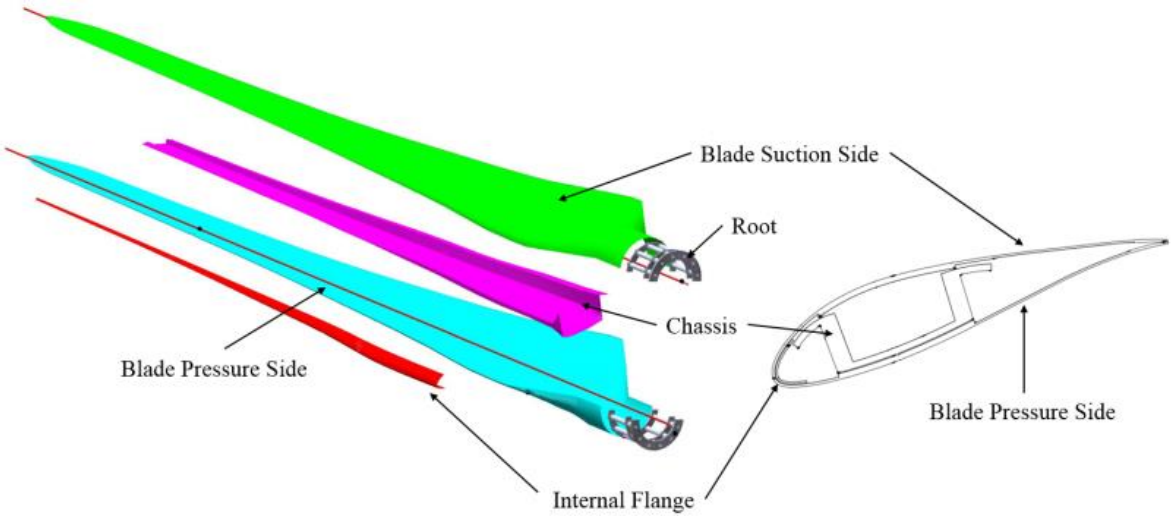

Figure 1. Blade assembly for 5-meter RUZGEM wind turbine blade [8].

2. Methodology

For the strength analysis of the blade, Puck and Tsai-Wu Failure Criteria, which are explained briefly in the following paragraphs are used.

Puck failure criteria [12] are one the most commonly used and well-established criteria for the assessment of composite laminate strength. Puck’s failure criteria are implemented for the evaluation of stress results of unidirectional and tri-axial laminate composite materials. For fiber failure, Puck’s criteria are as follows:

$$f_{E(FF)}^{T} = \frac{\sigma_1}{X_T} = 1 \tag{1}$$

$$f_{E(FF)}^{C} = \frac{\sigma_1}{X_C} = 1 \tag{2}$$

where $f_{E(FF)}^{T}$ and $f_{E(FF)}^{c}$ are stress exposures for fiber failure under tension and compression loading cases. σ_1 is the stress value in fiber direction, X_T and X_c are tensile and compressive strengths in fiber direction, respectively.

Puck's inter fiber failure criteria use the following equations:

$$f_{E(IFF)}^{A}=\left[\left(\frac{\sigma_6}{S}\right)^2+\left(1-p_{\perp II}^{(+)}\frac{Y_T}{S}\right)^2\left(\frac{\sigma_2}{Y_T}\right)^2\right]^{1/2}+p_{\perp II}^{(+)}\frac{\sigma_2}{S}=1 \tag{3}$$

$$f_{E(IFF)}^{B}=\frac{1}{S}\left\{\left[\left(\sigma_6\right)^2+\left(p_{\perp II}^{(-)}\sigma_2\right)^2\right]^{1/2}+p_{\perp II}^{(-)}\sigma_2\right\}=1 \tag{4}$$

$$f_{E(IFF)}^{C}=\left[\left(\frac{\sigma_6}{2(1+p_{\perp\perp}^{(-)})S}\right)^2+\left(\frac{\sigma_2}{Y_C}\right)^2\right]\frac{Y_C}{(-\sigma_2)}=1 \tag{5}$$

In the equations above $p_{\perp II}^{(+)}, p_{\perp II}^{(-)}$ and $p_{\perp\perp}^{(-)}$ represent inclination parameters that control the shape of the failure envelope. σ_2 is the stress value in the transverse fiber direction, Y_T and Y_c are tensile and compressive strengths in the transverse fiber direction. Shear stress and shear strength are represented by σ_6 and S, respectively. If the value of failure exposure (f_E) exceeds 1, failure initiation occurs. Mode A is caused by tensile and shear stresses. Modes B occurs under compressive and shear stresses. Mode C is a dangerous failure mode in compressive shearing which may lead to ultimate failure. Degradation rules are applied to the elements which fail according to the specific Puck's failure criteria that are inter fiber failure (IFF) mode A, B or C (Equations (3), (4) and (5), respectively). As presented in [4], based on degradation rules in Table 1, transverse elasticity and shear moduli of the failed elements are reduced accordingly.

Table 1: Degradation rules according to failure mode.

Failure Mode	Degradation Rule
IFF(A) & IFF(B)	$\mathrm{E}_2=\eta\times\mathrm{E}_2$
	$G_{12}=\eta\times G_{12}$
IFF(C)	$\mathrm{E}_2=0.1\times\mathrm{E}_2$
	$G_{12}=0.1\times G_{12}$

In Table 1 η is known as the degradation factor and can be expressed according to the equation below:

$$\eta=\frac{1-\eta_r}{1+c(f_{E(IFF)}-1)^{\xi}}+\eta_r \tag{6}$$

Recommended parameters c, η_r and ξ for the degradation function (6) are taken from [9]. $f_{E(IFF)}$ is the stress exposure value that is considered for determining the failure mode during the analysis.

ANSYS Parametric Design Language (APDL) is used to implement Puck's gradual failure process for the strength analysis of a composite laminate. Validation of the APDL Code against experimental data is done for the $[0/90]_s$ GFRP laminate/MY750 and $[0/\pm45/90]_s$ CFRP laminate/AS4 3501-6 under uniaxial tension loading [11]. As seen from Figure 2 there is a good agreement between APDL Code and experimental data for the progressive failure analysis of $[0/90]_s$ GFRP/MY750 and $[0/\pm45/90]_s$ CFRP/AS4 3501-6 laminates.

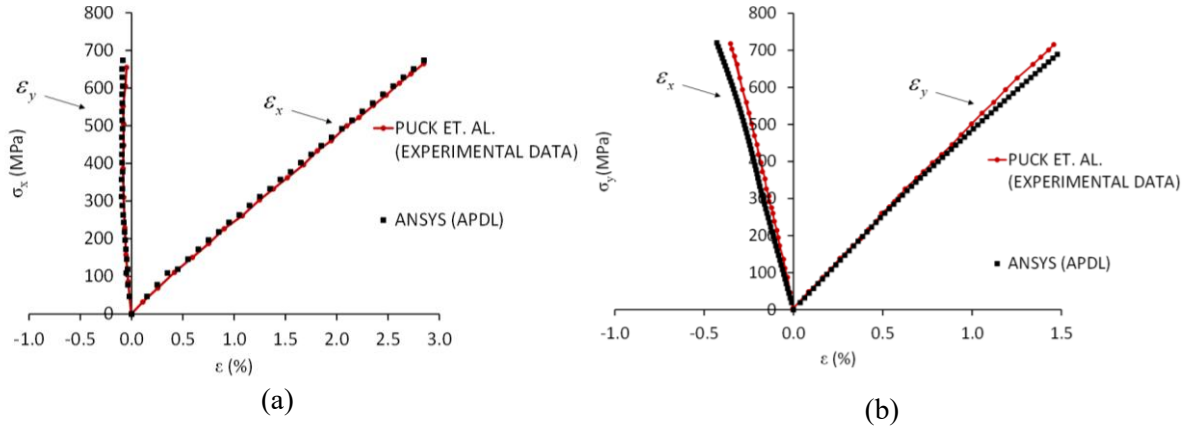

Figure 2. Validation of the APDL Code for the progressive failure analysis of (a) $[0/90]_s$ GFRP/MY750 laminate under σ_x uniaxial tension (b) $[0/\pm45/90]_s$ CFRP/AS4 3501-6 laminate under σ_y uniaxial tension.

Tsai-Wu failure criterion [15] is classified among fully interactive failure criteria expressed by the equation below:

$$\frac{\sigma_1^2}{X_t X_c} - \frac{\sigma_1 \sigma_2}{\sqrt{X_t X_c Y_t Y_c}} + \frac{\sigma_2^2}{Y_t Y_c} + \left(\frac{\sigma_6}{S}\right)^2 + \left(\frac{1}{X_t} - \frac{1}{X_c}\right)\sigma_1 + \left(\frac{1}{Y_t} - \frac{1}{Y_c}\right)\sigma_2 = 1 \qquad (7)$$

In equation (7), if the value of equation exceeds one, failure of the ply occurs. It is not possible to determine failure modes with this criterion. For Tsai-Wu failure criterion inverse reserve factor is calculated, which is a measure of failure level and is the equivalent terminology for failure exposure in Puck criteria.

3. Finite Element Modelling

The two-dimensional blade drawings which include the blade aerodynamic design details such as cord length and twist angle along the blade were provided by the blade manufacturer Compblades. By using these given two-dimensional blade drawings, the three-dimensional geometric modelling of the blade is performed in NX 10.0 environment.

Table 2 lists the experimental material properties of the blade materials [10].

Table 2. Material properties

Material Property		Unidirectional Laminate	Steel	Gel Coat	CSM 300	Divinycell H45
Density, ρ	[kg/mm^3]	1896	7850	1200	1896	200
Thickness, h	[mm]	0.716	5.3	0.9	0.358	5 or 10
E_1	[GPa]	12.17	210	1.95	4.47	0.269x10^{-3}
E_2	[GPa]	4.47				
ν_{12}		0.14	0.3	0.17	0.14	0.2
G_{12}	[GPa]	1.38				7.35 x10^{-3}
X_T	[MPa]	191.73	581.8	35.29	16.86	1.4
X_C	[MPa]	101.16				0.6
Y_T	[MPa]	16.86				1.4
Y_C	[MPa]	50.41				0.6
S	[MPa]	11.29				0.56

The skin of the blade is composed of unidirectional and tri-axial laminates. The lay-up sequence for the pressure and suction side differs only in the area from 1.25m to 2.0m where an additional unidirectional glass fabric was placed in the suction side of the blade. The root part of the blade is composed of unidirectional laminate, tri-axial laminates and steel. The outer surface of the blade is covered with transparent Gel Coat and a layer of chopped strand mat, 300 g/m^2 CSM 300. Additionally, The Divinycell H45 foam used in the trailing edge is of 10 mm thickness in the area from 0.7m to 2.0m

and 5mm thickness from 2.0m to 3.0m. Since gel coat and foam do not have a significant contribution to the strength of the blade, these materials are neglected in finite element model.

After geometric modeling of the blade, the material model of the blade structure is built using Ansys ACP/Pre module. Due to different lamination plan for different blade sections, the thickness of the blade skin varies along the blade. The composite layer thickness in the aeroshell of the blade changes as seen in Figure 3 from the root to the tip of the blade.

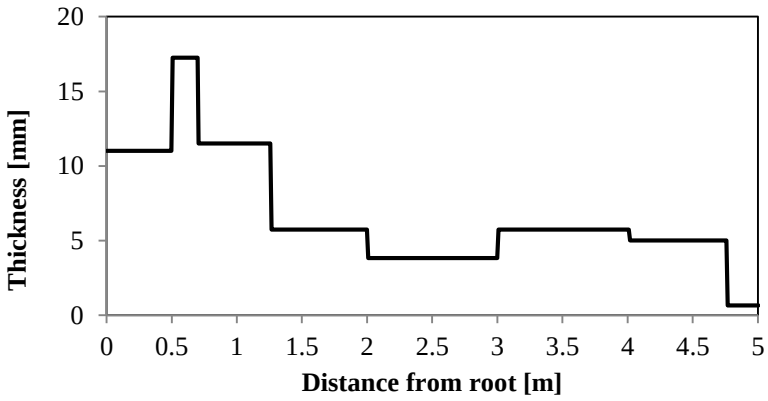

Figure 3. Layer thickness for the composite aeroshell of the blade.

After material modelling of the blade was finished in Ansys ACP, the blade was meshed entirely with 20,013 layered shell elements and 42,975 nodes in ANSYS Workbench as seen in Figure 4. The fine mesh density was chosen on the blade training edges for detailed investigation of the stress distribution in these areas.

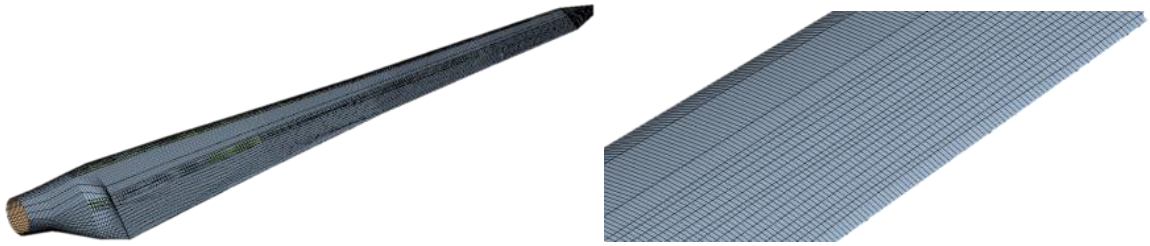

(a) (b)

Figure 4. (a) The mesh of the aeroshell, (b) the close-up view of the tip of the blade.

The turbine specifications are obtained from the meteorological data in Ankara. These were analyzed so that, average wind speed, occurrence of gusts and wind speeds are determined. Based on this information the turbine specifications were selected according to IEC 61400-2 standard [7]. Worst case load scenario is chosen among the complete set of IEC extreme loads provided from aero-elastic simulations. The extreme loads are computed using the wind turbine aero-hydro-servo-elastic software tool FAST version v7.01.00a-bjj. During the simulations the turbine is simulated as a stall regulated constant speed turbine at 83 rpm with a gearbox and simple induction generator. Using this data, the blade is analysed under extreme loads in the flapwise direction including a safety factor of 1.35, which is presented in Figure 5. Flapwise forces are placed at 21 stations along the blade.

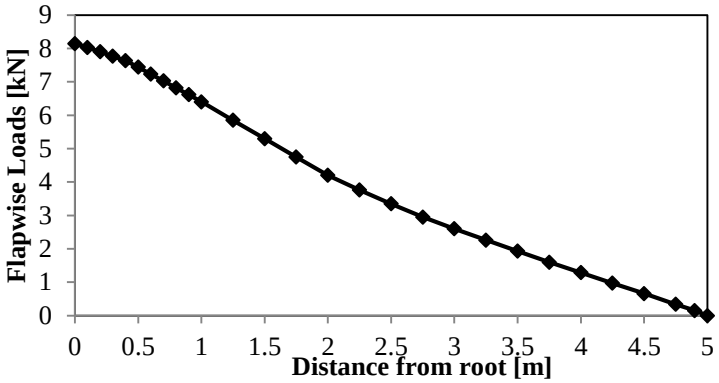

Figure 5. Load distribution along span length.

4. Results and discussion

In this study, blade failure was modelled using three different composite failure models: linear elastic analysis using Tsai-Wu criteria, linear elastic analysis using Puck criteria and progressive failure analysis using Puck criteria. In Figure 6, load displacement curve of the existing composite blade is given for the linear model (Puck and Tsai-Wu) and nonlinear model (progressive Puck) for loads corresponding to 20%, 30%, %40 and 50% of extreme flapwise loading. Up to 30% of the extreme flapwise loading, the stiffness for both models are seen to be the same (Figure 6). Yet, after 30% of extreme flapwise loading, difference in stiffnesses starts to be noticeable, and at 50% of extreme flapwise loading the difference in stiffness of blade reaches its maximum level. At this point the deflection of the nonlinear model is more than 1.5 times the deflection of the linear model and the blade is considered to be close to ultimate failure. Hence, the simulation was stopped at 50% of loading. The results given in this section are limited to 50% of extreme flapwise loading.

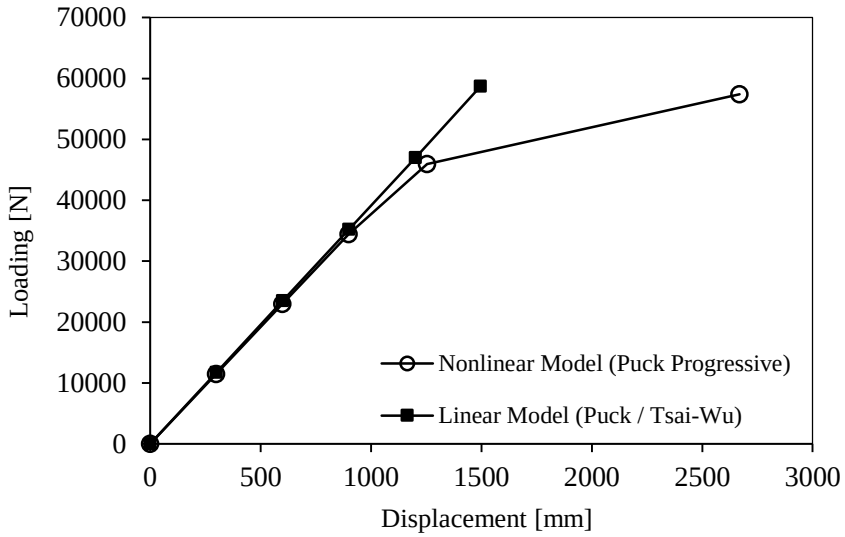

Figure 6. Load displacement curve of the blade corresponding to linear model (Puck / Tsai-Wu) and nonlinear model (Puck progressive).

In this section, contour plots of the failure inverse reserve factor in the suction side of the blade is presented for loads corresponding to 20%, 30%, %40 and 50% of extreme flapwise loading. Since suction of part of the blade is heavily damaged under extreme flapwise loading, our focus of investigation is the suction part. Figure 7 shows contour plots of Tsai-Wu failure inverse reserve factors for loads corresponding to 20%, 30%, %40 and 50% of extreme flapwise loading. Failure occurs if

inverse reserve factor is greater than 1 and these failure areas are indicated in red. At 20% load, failure initiation begins at two main regions: interface between chassis-skin and part of the skin close to trailing edge. When 30% load level is reached, the failed region propagates along the interface between the chassis-skin, root and part of the skin close to trailing edge and leading edge. Under 40% and 50% of loading, we observe from the figure, that as the loading is increased incrementally, failed regions cover a larger area of the blade.

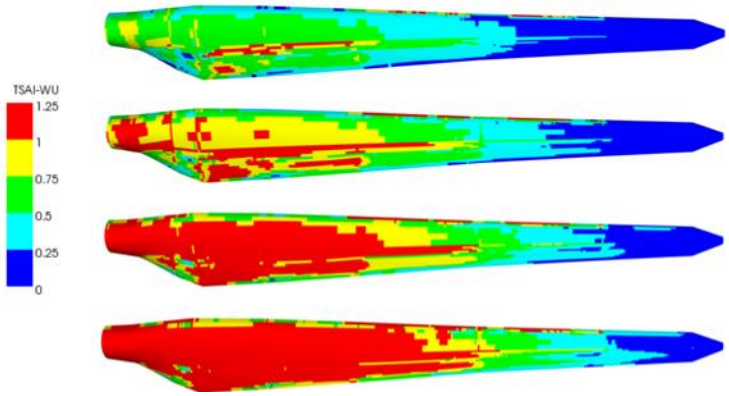

Figure 7. Contour plots of Tsai-Wu failure reserve factors at 20%, 30%, %40 and 50% of extreme flapwise loading.

When Puck failure criteria are considered, ultimate failure of the blade is considered to take place if fiber failure (FF) in any ply occurs or when inter fiber failure IFF (C) in more than three plies of a laminate is observed. FF reduces the structural strength of the composite part drastically due to high energy release. In addition, risk of delamination is high when IFF (C) is seen in all plies [4].

Figure 8 and Figure 9 show contour plots of Puck failure exposures for IFF(A), IFF(B) (inter fiber failure modes A and B) in suction side of the blade under static loading in flapwise direction, respectively. Failure exposures greater than 1 represent elements that need to be degraded and these elements are depicted in red. In the suction side of the blade, failure exposures of IFF(A) and IFF (B) modes initiate in the root and trailing edges of the blade at 20% and 30% of loading. As the loading is further increased to 40% and 50% degraded regions at the root and trailing edge become larger. In the progressive Puck model, failure pattern expands over a larger area under 40% and 50% of loading compared to linear model. This situation is caused mainly due to the failed elements as a result of FF (fiber failure) and IFF(C) (inter fiber failure mode C) (Figures 10 and 11). The dark blue regions in the middle of red regions represent elements, which were failed due to FF and IFF(C). These elements do not contribute the stiffness of the blade anymore and they do not carry load. Failure modes IFF(A) and IFF(B) are dominant over a larger area compared to FF and IFF(C). However, since IFF(A) and IFF(B) do not cause ultimate failure, these modes are not treated as critical as FF and IFF(C).

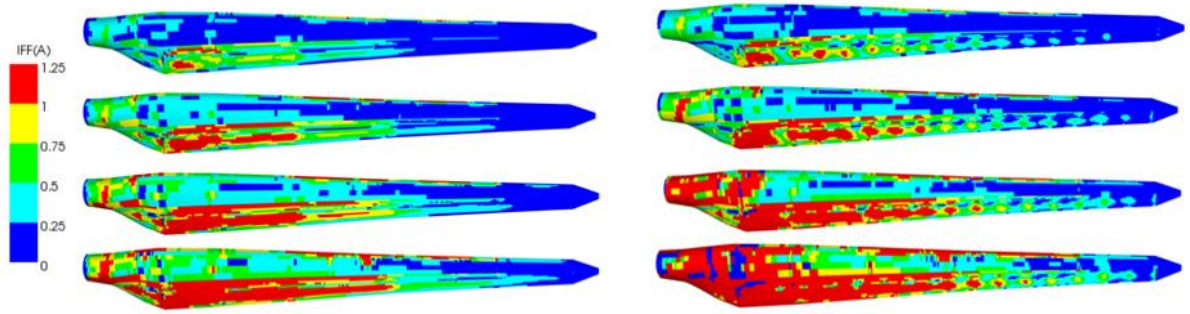

(a) (b)

Figure 8. Contours of IFF (A) modes for the suction side of the blade using (a) Linear Puck Criteria (b) Progressive Puck Criteria at 20%, 30%, 40% and 50% of extreme flapwise loading.

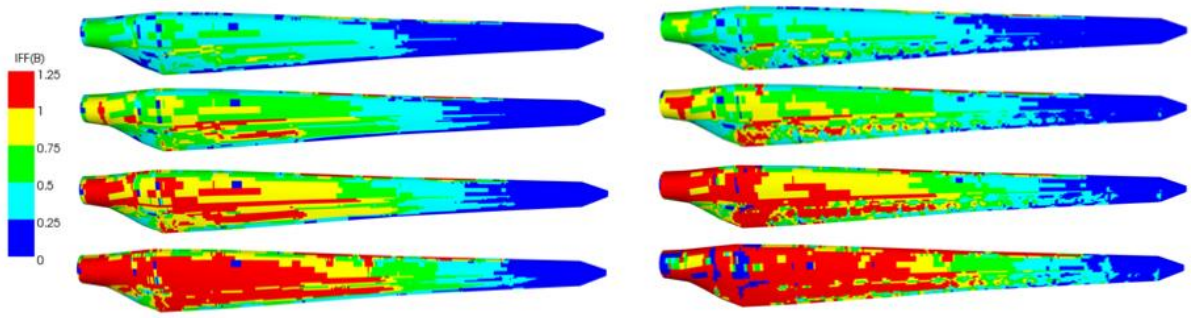

(a) (b)

Figure 9. Contours of IFF (B) modes for the suction side of the blade using (a) Linear Puck Criteria (b) Progressive Puck Criteria at 20%, 30%, 40% and 50% of extreme flapwise loading.

In a similar manner, Figure 10 and Figure 11 show contours of IFF(C) and FF for 20%, 30%, 40% and 50% of the extreme load case in flapwise direction. As seen from the figures failure of elements due to FF and IFF(C) become visible at 30% loading. In the analysis, where progressive Puck failure criteria are used, the stiffness of the elements which are failed at 30% loading are set to zero. These elements do not contribute to the stiffness of the blade afterwards. This situation becomes visible at 40% loading. The failed regions appear as dark blue regions in the middle of red regions. Dark blue regions represent regions, where elements do not carry load and their stress values are zero. Hence, their failure exposures are zero, as well. As it was the case for IFF(A) and IFF(B) in the progressive failure analysis failure expands over a larger area starting from 30% loading. This result is in agreement with load displacement curve in Figure 6, where we start to observe stiffness reduction. Another observation, which can be drawn from the investigation of Figure 10 and Figure 11 is that, load paths and failure pattern change as the elements fail after 30% loading. We see that due to failure of elements in progressive analysis, trailing and leading edges of the blade are subjected to more loading than in the linear model. These regions are now under high risk of failure. The aforementioned results allow us to come the conclusion that, progressive failure analysis is necessary in order to capture a more realistic simulation of the failure mechanisms prior to testing.

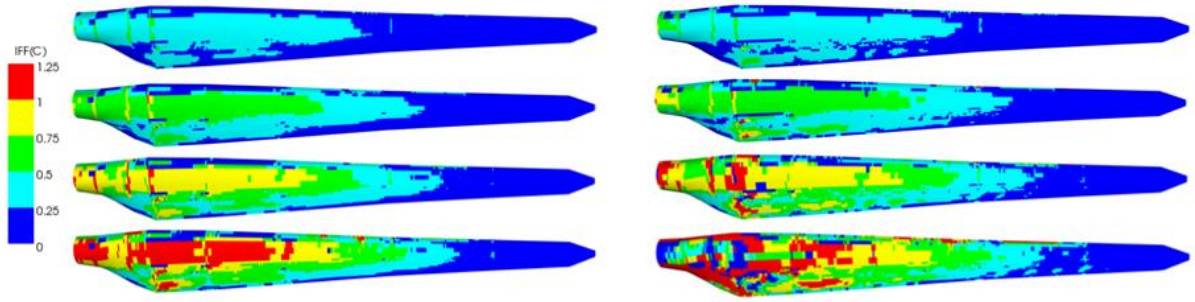

(a) (b)

Figure 10. Contours of IFF (C) modes for the suction side of the blade using (a) Linear Puck Criteria (b) Progressive Puck Criteria at 20%, 30%, 40% and 50% of extreme flapwise loading.

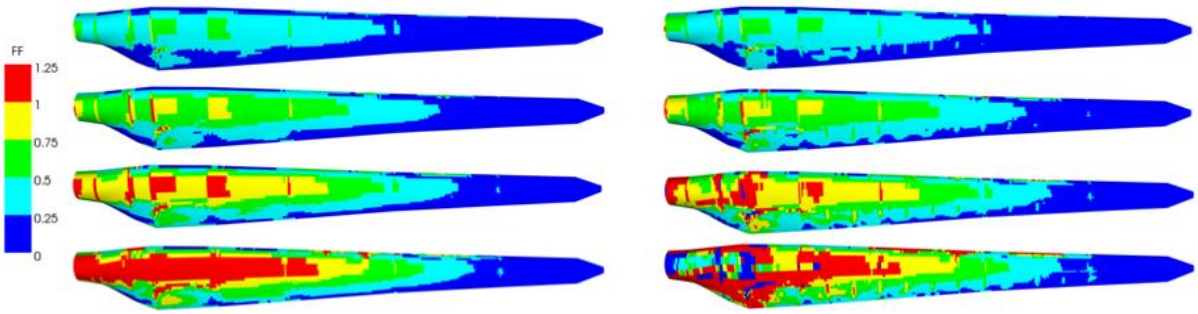

(a) (b)

Figure 11. Contours of FF modes for the suction side of the blade using (a) Linear Puck Criteria (b) Progressive Puck Criteria at 20%, 30%, 40% and 50% of extreme flapwise loading.

As stated in Fagan et. al. [13], we also note that, the degradation in the shear and transverse material stiffness does have an important effect on the deflection of the blade. Only after elements begin to fail due to FF or IFF(C) starting from 30% loading, significant drop in the load displacement curve in Figure 6 becomes apparent.

When Tsai-Wu and Puck failure criteria for the strength evaluation of the blade are compared, we see that failure initiation and progression patterns are similar only in IFF(B) case. For the Tsai-Wu failure criterion, failed regions are observed to be larger compared to the case when Puck criteria are used.

In the suction side of the blade, significantly high failure modes are concentrated mainly in the root and trailing edges of the blade for all three composite failure models. In particular the failure exposures observed at the 0.7 meter from the root of blade prevents us from satisfying the strength and stiffness requirements. Thus, the detailed cross sectional Von-Mises stress distributions in chordwise direction for both linear and nonlinear model at the 0.7 m from the root of blade are investigated in Figure 13 under 50% loading. In Figure 12 stress distributions in suction and pressure side in chordwise direction are displayed. Stress distributions for chassis and internal flange are displayed in Figure 13 (a) and (b), respectively. In general, stresses in the nonlinear model are higher than the stresses in linear model. Besides this, the stress peaks differ between linear and nonlinear model. We observe from the figures that the stress values at failed elements are zero.

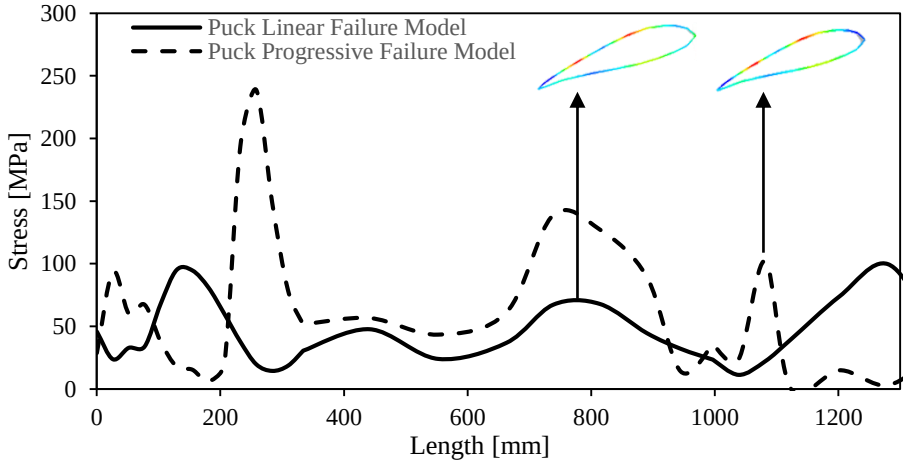

Figure 12. Von-Mises stress distribution at 0.7 m from root blade skin (Suction and pressure side).

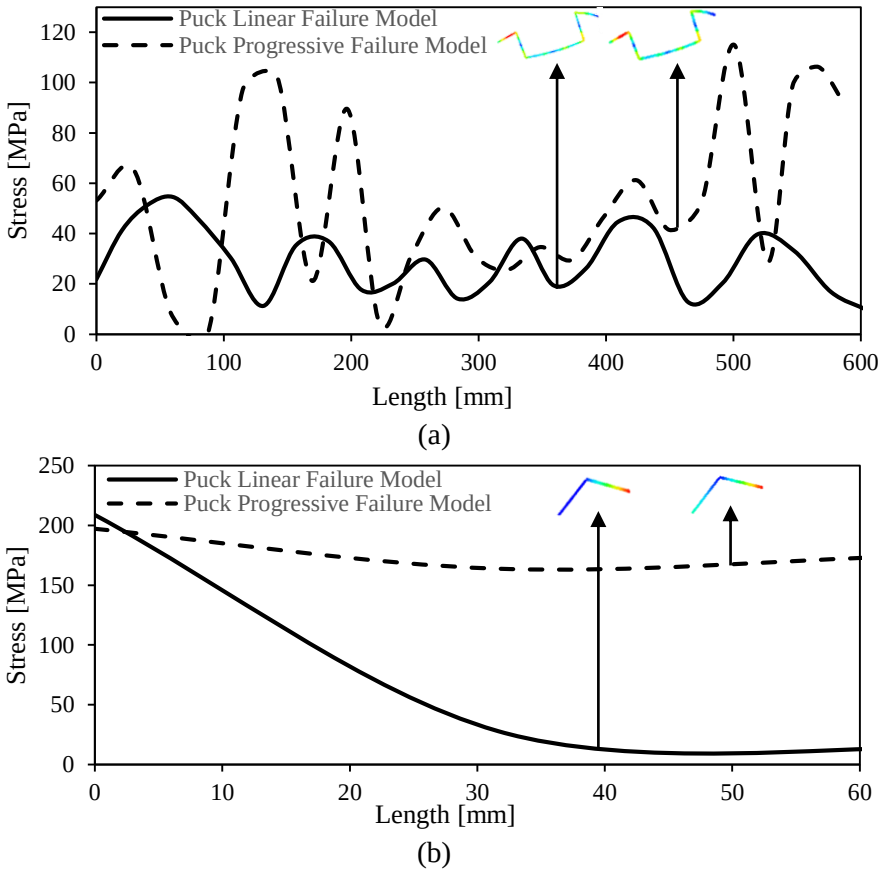

Figure 13. Von-Mises stress distribution at 0.7 m from root (a) Chassis (b) Internal flange.

During its operation a wind turbine blade is subjected to large edgewise and flapwise bending moments. These moments induce stresses in aeroshell, adhesive joints and spar of the blade. Stress states vary with position in the blade and within a cross-section [2]. Typical failure modes observed when a blade was tested is depicted by Sorensen et al. [14]. In their paper, adhesive joint failure is observed at the leading and trailing edges. In addition to this, skin/adhesive debonding and delamination is observed between the layers of the aeroshell. Likewise, strength analysis of the 5-meter RUZGEM wind turbine blade shows that failure exposures are particularly high at the leading, trailing edges and at the interface chassis-skin, where we expect that failure initiation will begin. IFF(A, B and C) are expected to facilitate delamination at these locations. Fagan et. al. [13] pointed out that blade root is subjected to high stresses due to bending moment and, hence blade root plays an important role as a design driver. Similarly, high failure exposures are computed at the root of RUZGEM blade.

5. Conclusions

In this work, the strength of an existing 5-meter composite wind turbine blade under extreme flapwise loading condition is analyzed using Tsai-Wu and Puck failure criteria in order to predict failure modes and failure exposures before testing. The conclusions are as follows:

1. Failure of elements are observed and the blade is found to deflect excessively under 50% of the extreme load case, ultimate failure is expected to occur and the blade needs to be redesigned.
2. In the analysis, linear material model using Tsai-Wu and Puck criteria are compared with the nonlinear model using progressive Puck criteria. When Tsai-Wu failure criterion is used failed regions are seen to be larger compared to the case when Puck criteria are used. The load paths and failure pattern change as the elements fail when progressive Puck criteria are

used. Hence, progressive failure analysis is necessary in order to capture more realistic simulation of the failure mechanisms prior to testing.

3. Load displacement curves of the blade under extreme flapwise loading are plotted. Stiffness reduction of the curve becomes notable only after failure of elements due to IFF(C) and FF. Shear and transverse stiffness reductions due to IFF(A) and IFF(B) do not lead to significant changes in the overall load displacement behavior of the blade.
4. Strength analysis of the blade using Puck failure criteria is useful for predicting failure initiation load, failure mode and failure location before testing of the blade. This failure analysis will help to calibrate the blade test set-up.

Acknowledgement
This work was partly supported by RUZGEM, METU Center for Wind Energy at the Middle East Technical University.

References

[1] DNV Standard 2010 *DNV-OS-J102 - Design and manufacture of wind turbine blades*
[2] J. W. Holmes, B. F. Sørensen, P. Brøndsted 2007 *Reliability of wind turbine blades: an overview of materials testing* Wind Power Shanghai (1-3 November 2007)
[3] E. M. Fagan, C. R. Kennedy, S. B. Leen, J. Goggins 2016 *Damage mechanics-based design methodology for tidal current turbine composite blades* Renewable Energy 97 358-372
[4] V.A. Passipoularidisa, T.P. Philippidis, P. Brondsted 2011 *Fatigue life prediction in composites using progressive damage modeling under block and spectrum loading* International Journal of Fatigue 33 132–144
[5] C. Kong, J. Banga, Y. Sugiyama, 2005 S*tructural investigation of composite wind turbine blade considering various load cases and fatigue Life* Energy, 30 p 2101
[6] F.M. Jensen, B.G. Falzon, J. Ankersen, H. Stang 2006 S*tructural testing and numerical simulation of a 34 m composite wind turbine blade* Composite Structures 76 p 52
[7] British Standard 2006 *Wind Turbines, Part 2: Design requirements for small wind turbine* BS EN 61400-2:2006
[8] T. P. Philippidis, G. A. Roukis 2013 *Structure design report of METUWIND small rotor Blade* Confidential Interim Report
[9] M. Knops, C. Bögle 2006 *Gradual failure process in fiber/polymer laminates* Composites Science and Technology, special issue on Composite Materials Reliability and life prediction of composite structures 66 616-625
[10] T. P. Philippidis, T. T. Assimakopoulou, G. A. Roukis 2013 *Static tests on GFRP composites made of METYX Glass NCF* Confidential Interim Report
[11] A. Puck, H. Schuermann, 2002 *Failure analysis of FRP laminates by means of physically based phenomenological models* Composite Science and Technology 621633-1662
[12] M. Knops, 2008 *Analysis of failure in fiber polymer laminates the theory of Alfred Puck* ISBN 978-3-540-75764-1
[13] E. M. Fagan, S. B. Leen, C. R. Kennedy, J. Goggins 2015 *Finite element-based damage assessment of composite tidal turbine blades* Journal of Physics: Conference Series 628 012106
[14] B. F. Sørensen, K. Branner, H. Stang, H.M. Jensen, E. Lund, T.K. Jacobsen and K.M. Halling, 2005 *Improved Design of Large Wind Turbine Blades of Fibre Composites (Phase 2) – Summary Report* Risø National Laboratoty Roskilde Denmark Risø-R-1526(EN)
[15] S. Tsai, M. Wu, M. 1971 *A General Theory of Strength for Anisotropic Materials*, J. Composite Materials, Vol. 5.